Nuclear Instruments and Methods in Physics Research A 628 (2011) 444–447

Contents lists available at ScienceDirect

Nuclear Instruments and Methods in Physics Research A

journal homepage: www.elsevier.com/locate/nima

The ClearPEM breast imaging scanner

Jorge A. Neves

Laboratório de Instrumentaçao e Física Experimental de Partículas (LIP), Lisbon, Portugal

On behalf of the ClearPEM Collaboration

ARTICLE INFO

Available online 6 July 2010

Keywords:
Positron emission mammography
Avalanche photodiodes
Front-end electronics
Application-Specific Integrated Circuit (ASIC)
Energy and time resolution
Image reconstruction

ABSTRACT

We present results on the characterization of the ClearPEM breast imaging scanner. ClearPEM is a dual-head positron emission mammography scanner using APD-based detector modules that are capable of measuring the depth-of-interaction (DOI) with a resolution of 2 mm in LYSO:Ce crystals. The full system comprises 192 detector modules with a total of 6144 LYSO:Ce crystals and 384 32-pixel APD arrays read out by ASICs with 192 input channels. The scanner includes front-end and data acquisition electronics and a robotic gantry for detector placement and rotation. The software implements calibration (energy, time and DOI), normalization and image reconstruction algorithms.

In this conference, the scanner main technical characteristics, the calibration strategies and the spectrometric performance in clinical environment were presented as well as the images obtained with point sources and with a microDerenzo phantom. The image resolution was found to be of the order of 1.3 mm FWHM (center of field-of-view) and the DOI capability has shown to have a strong impact on the image sharpness. An assessment of the first clinical experience was also presented at the conference.

1. Introduction

Breast cancer is the most common cancer affecting women, with an incidence rate of about 1.2 million females per year worldwide. Positron emission tomography has demonstrated large potential for cancer detection since the radiotracer injected into the patient fixates in tumor cells and its biodistribution can be measured by the temporal coincidence detection of the 2γ photons resulting from the positron–electron annihilation when the radiotracer decays. Here is presented the ClearPEM—a breast cancer imaging scanner developed by the Portuguese PET consortium under the framework of the Crystal Clear Collaboration [1].

2. The ClearPEM scanner

The ClearPEM is a dual-head positron emission tomography scanner that uses APD-based detector modules in a double-readout scheme for the DOI measurement in LYSO:Ce crystals. The DOI coordinate is determined from the asymmetry of the light collected on the two APD pixels reading out the same crystal. The detector module performance allows to measure the photon interaction coordinate along 20 mm crystals with a resolution of 2 mm FWHM [2]. This reduces the degradation of the spatial resolution due to the parallax effect, in particular when the scanner operates at smaller separation distance between the detectors (8–10 cm) in order to increase the photon detection acceptance. We had investigated the influence of the DOI resolution on reconstructed images using simulated data and had concluded that a 2 mm DOI resolution allows to achieve an image spatial resolution of about 1.2 mm [1].

The detector module consists on 32 LYSO:Ce crystals with $2\times2\times20\,mm^3$ arranged on a 4×8 matrix made of $BaSO_4$ walls. It is optically coupled on both ends to APD arrays that can be assembled in a planar arrangement within the detector heads. Such a planar geometry is rather flexible and can easily accommodate different breast sizes by simply positioning the detector heads at different separation distances and rotation angles. For that purpose, we developed a supermodule structure that groups 12 detector modules placed between a top and a bottom front-end electronic board [3]. Each ClearPEM detector head has eight of these supermodules (covering an active area of $16\times18\,cm^2$) and a Service Board that provides low and high voltage power supply, slow control signal distribution and APD's temperature monitoring.

The APDs are kept at 18 °C by a water cooling system and the readout is performed by a dedicated ASIC with 192 input channels. To deal with signals from low gain APDs, the ASIC

E-mail address: janeves@lip.pt

0168-9002/$ - see front matter © 2010 Elsevier B.V. All rights reserved.
doi:10.1016/j.nima.2010.07.021

performs low noise pulse amplification (*ENC* 1300 e^-) and shaping (40 ns rise time) [4]. The amplifiers' output signals above the threshold voltage are stored in analog memories that are then multiplexed in two output channels (to allow the readout of Compton events). In parallel, a digital channel ID identifies the crystal position from where the pulse came out.

Each front-end board is equipped with two ASICs and is also responsible for the data analogue-to-digital conversion by two high-speed dual ADCs (10 bits, 50 MHz) and for the communication to the off-detector data acquisition electronics by one LVDS channel link transmitter (2.4 Gbps).

The digital data coming from the detector heads' front-end electronics goes to the off-detector data acquisition electronics that is responsible for digital data processing, in order to identify coincidences and to send meaningful data to the acquisition server for further event processing. This system is composed of four DAQs (Data Acquisition Boards—Slaves) that receive digital data through the LVDS channel link transmitter. The DAQ's FPGA finds top–bottom crystal coincidences and sends relevant data to the TGR-DCC (Trigger and Data Concentrator Board—Master). The TGR-DCC's FPGA looks for 511 keV photons in coincidence between two detectors heads and the data are sent to the acquisition server by a SLink bridge.

The ClearPEM scanner was installed at the Instituto Português de Oncologia, Porto, to be used in breast cancer detection clinical trials. The ClearPEM scanner comprises a robotic gantry, the detector heads and the examination table for the patient to lie prone. The robot controls the rotation and the separation distance between the detector heads. The two detector heads can be rotated by 90° to allow imaging of the axial region.

3. Detector calibration

The energy of photon hits is given by the sum of the energies measured by the two APDs that readout the top and bottom ends of the crystal where the photon interacted. It is then required that both APDs have an equalized gain. Taking advantage of the natural presence of ^{176}Lu within the LYSO:Ce crystal, uniformly distributed along its entire volume, the inter-pixel gain is determined by assuming that the spectrum of each APD is the same. The absolute crystal calibration is obtained by identifying the position of the 511 keV peak on the summed spectrum. The DOI calibration constant, that transforms the ratio of shared light into a physical distance, is obtained using the ^{176}Lu natural radiation. This constant is determined by finding the edges of the asymmetry distribution and assuming that it corresponds to the crystal extremities.

4. Energy and time resolution

As described before, the APD signals are amplified and sampled at 50 MHz in a dedicated ASIC [4]. The pulse data-frame is composed of 10 samples sent to the off-detector trigger and data acquisition system which computes the energy and time of individual crystal hits. When a coincidence event is identified, the selected data are then stored in a disc [5]. A key assumption for the time extraction of each pulse is that the average pulse shape for every APD channel is predetermined. The pulse reconstruction of the individual channels is obtained by fitting the average pulse shape to a function with two parameters, namely the peaking time and the time decay constant.

Energy measurements from the coincidence events show that the scanner presents a good energy linearity and that the energy resolution and the photopeak position are not dependent on the depth-of-interaction of the photon in the crystal.

The sum of the spectra of all crystals after the detector calibration is shown in Fig. 1. The overall scanner energy resolution is 16%. The distribution of the energy resolution at 511 keV measured individually for all channels is shown in Fig. 2, presenting a mean value of 15.9% and a dispersion of 8.8%, extracted from a Gaussian fit. We can also conclude that it is possible to obtain with the double-readout configuration an energy resolution similar to those obtained with single-readout schemes with multi-anode PMTs or with multi-pixel APDs systems.

In the top–bottom event energy scatter plot shown in Fig. 3 we can clearly distinguish the Compton region and the 511 keV peak. The 511 keV peak shows a greater number of high energy events read by the bottom APDs, which can be explained by the fact that most of the photons interact near the crystals bottom face as this one is closer to the radiation source.

The coincidence time resolution for 511 keV photons, defined as the FWHM of the Gaussian fit of the distribution of the time difference between any two hits in opposite detector heads, using a 400–600 keV energy window, is of 5.2 ns as shown in Fig. 4. Such a low value for a compact, dual-readout APD-based system is the result of the very low noise level achieved in the front-end electronics and the careful optimization of the detector modules [6].

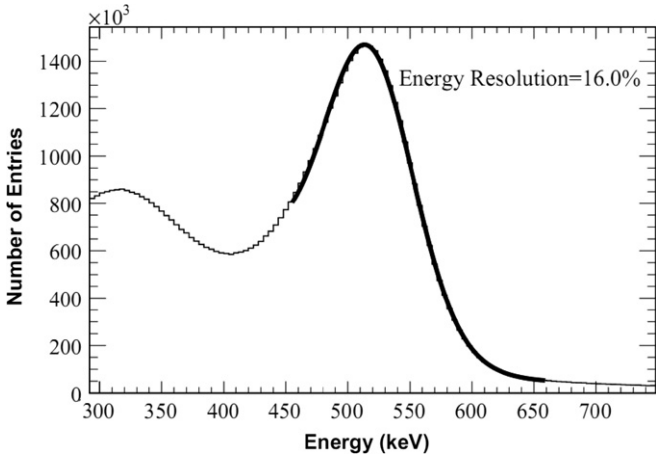

Fig. 1. Summed energy spectra of all crystals. The overall scanner energy resolution is 16%.

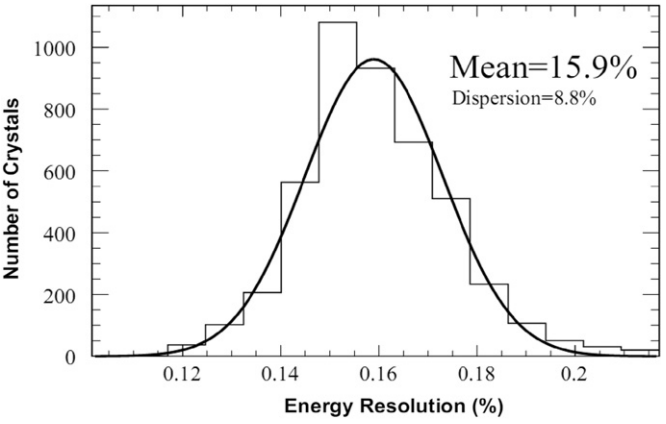

Fig. 2. Energy resolution at 511 keV for all channels.

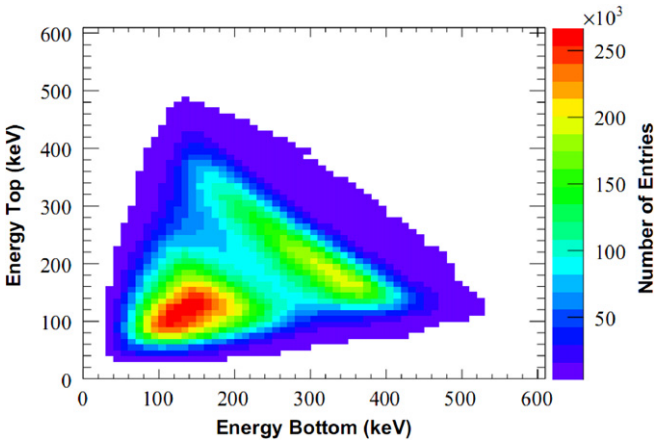

Fig. 3. Scatter plot of the crystals top *vs* bottom event energy deposition.

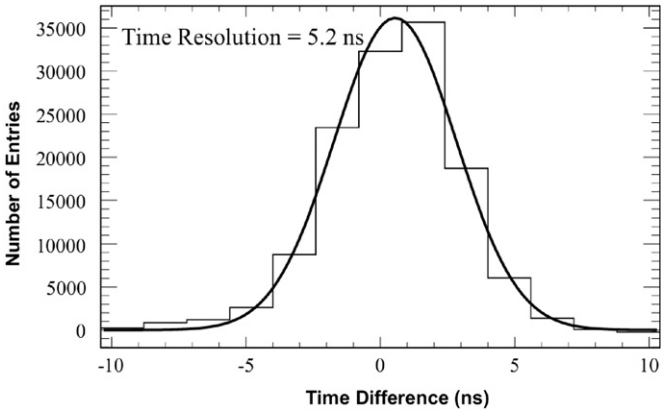

Fig. 4. Distribution of the measured time differences between any two hits in opposite detector heads, using a 400–600 keV energy window.

5. Image reconstruction

The STIR library [7] was used as a base platform for the 3D image reconstruction for the ClearPEM scanner. Classes were introduced in the library to deal with the planar nature of the ClearPEM scanner [8]. The software has been updated to accommodate different distances between the detector plates and angular acquisition positions.

In order to evaluate the imaging performance of the scanner, a ^{22}Na point source (1 mm) was used to scan a 4×4 grid with 5 mm pitch in the scanner's field-of-view. The data from the 16 positions were sequentially acquired in list mode and later were merged in a single sinogram used by the reconstruction algorithms. For each coincidence event the LOR (line-of-response) is computed taking into account the x–y–z coordinates of the photon hits as given by the crystal index and the DOI measurement. The images shown in Fig. 5 were obtained with the algorithm 3D-OSEM. Fig. 5 (left) shows the individual sources well resolved, with a FWHM of about 1.6 mm. Deconvoluting the source diameter of 1 mm we estimate a point resolution of 1.3 mm FWHM at the center of the field-of-view. Fig. 5 (right) shows the same data reconstructed without making use of the DOI information for each hit. In this case the LORs are computed using the x–y coordinates of the crystal pixels and assuming the coordinate z at the front face of the crystals. A considerable blurring of the image is observed.

The imaging performance of the scanner was also evaluated using a sealed microDerenzo phantom filled with ^{22}Na gel (20 μCi activity) with rods of 1.2, 1.5, 2.0, 2.5, and 3.0 mm diameter and a center-to-center distance between adjacent rods that is twice the rod diameter. Fig. 6 shows the acquired image using a 150 mm separation between the detector heads, 450–600 keV and 6 ns energy and time windows. Although no attenuation, Compton or random corrections were performed, the scanner can resolve rods below 2 mm diameter what is compatible with the required spatial resolution.

Fig. 7 shows one of the first images of a clinical breast exam performed on patients without breast lesions. The PEM exam was carried through four angular orientations, 150 mm between the detector heads and for a coincidence window of ± 4 ns, an energy window of 400–650 keV, and after a normal PET/CT examination profiting from the remaining FDG tracer activity. Although the breast image has no lesion indication, the shaping of the breast is clearly seen. Data from a ^{22}Na source were superimposed at sinogram level emulating a small lesion with a ratio to background of around 4. No attenuation, Compton or random corrections were performed, and the fraction of randoms in the field-of-view is about 35%.

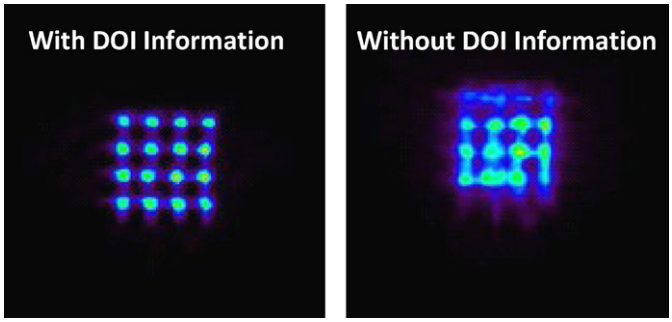

Fig. 5. Reconstruction (3D-OSEM) of the 4×4 ^{22}Na sources of 1 mm forming a grid with 5 mm pitch, and study of the influence of the DOI information on the reconstructed images (left and right).

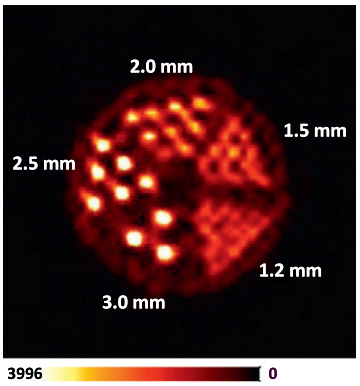

Fig. 6. Reconstruction (3D-OSEM) of the Derenzo Phantom.

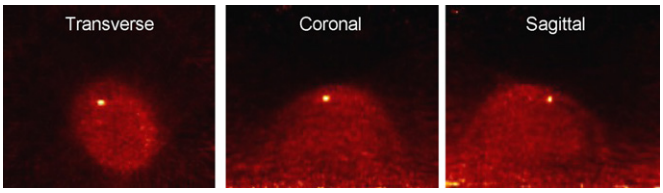

Fig. 7. Image of a clinical breast exam superimposed at sinogram level with data of a ^{22}Na source emulating a small lesion with a ratio to background of around 4.

6. Conclusions

The ClearPEM scanner was presented on the 12*TH Vienna Conference on Instrumentation*. An unprecedented integration of a large number of APD channels in high gain and compact, low noise front-end boards was achieved, together with the successful development of a mechanical robotic structure, data acquisition electronics plus detector control and safety systems. The results show homogeneous light collection for a uniform irradiation, 15.9% energy resolution at 511 keV with 8.8% dispersion and a FWHM coincidence time resolution of 5.2 ns. This allows a precise identification of positron annihilation coincidence events and the measurement of the photon interaction position in the crystal with a DOI resolution of at least 2.2 mm. It was shown that the optimization carried out to extract DOI information, while enabling better reconstructed images, does not compromise the overall energy and time resolution, which are similar or better than PET systems based in PMT-readout. The image resolution measured with point sources is of the order of 1.3 mm FWHM (center of field-of-view). The DOI capability was found to have a strong impact on the image sharpness. A first assessment of the clinical experience was presented at the conference.

Acknowledgements

The author would like to thank colleagues from the Portuguese PET Consortium and the Crystal Clear Collaboration. The author's work is supported by FCT (Fundaçao para a Ciência e Tecnologia) under the Grant SFRH/BD/33667/2009, and the ClearPEM project is financed by Adi (Agência de Inovaçao) and FCT/POSI (Programa Operacional Sociedade de Informaçao), Portugal.

References

[1] M.C. Abreu, et al., IEEE Trans. Nucl. Sci. NS-53 (1) (2006) 71.
[2] P. Amaral, et al., Nucl. Instr. and Meth. A 580 (2007) 1123.
[3] A. Trindade, et al., Performance evaluation of a highly integrated APD/ASIC double-readout supermodule with 768 channels for clear-PEM, IEEE Nuclear Science Symposium Conference Records, 2008.
[4] E. Albuquerque, et al., Nucl. Instr. and Meth. A 598 (2009) 802.
[5] R. Bugalho, et al., Experimental validation and performance analysis of the clear-PEM data acquisition electronics, in: IEEE NSS-MIC Conference Records, 2008.
[6] R. Bugalho, et al., JINST 4 (2009) P10011.
[7] 〈http://stir.sourceforge.net/〉.
[8] M. Martins, et al., Clear-PEM data reconstruction using STIR, Annual Congress of the European Association in Nuclear Medicine, Istanbul, October 2005.